Cureus Journal of Engineering

Open Access Original Article

Enhanced Photocatalytic Degradation of Rhodamine 6G Using Polypyrrole-ZnO Microcomposite Under UV Light Illumination

Received 05/13/2024
Review began 05/14/2024
Review ended 08/19/2024
Published 08/21/2024

© Copyright 2024
Satpal et al. This is an open access article distributed under the terms of the Creative Commons Attribution License CC-BY 4.0., which permits unrestricted use, distribution, and reproduction in any medium, provided the original author and source are credited.

DOI:
https://doi.org/10.7759/s44388-024-00033-4

Sudhakar B. Satpal [1] , Anjali A. Athawale [2]

1. Department of Chemistry, Haribhai V. Desai College of Arts, Science, and Commerce, Pune, IND 2. Department of Chemistry, Savitribai Phule Pune University, Pune, IND

Corresponding author: Anjali A. Athawale, dranjaliathawale@gmail.com

Abstract

This work presents the synthesis of microcomposites of polypyrrole (PPy) and zinc oxide (ZnO) in varied weight percentages (1, 2, and 5 wt.%) for their potential in photocatalytic reactions. The properties of composites were investigated thoroughly using sophisticated analytical techniques, viz. X-ray diffraction, Fourier-transform infrared spectroscopy, Raman spectroscopy, Field emission scanning electron microscopy, energy-dispersive X-ray spectroscopy, ultraviolet-visible spectroscopy, thermogravimetric analysis, and Brunauer-Emmett-Teller analysis. The stretching vibrations of the Zn-O and N-H bonds corresponded to distinctive band frequencies at 480 cm^{-1} and 588 cm^{-1}, respectively, as indicated by the Fourier-transform infrared spectra analysis. Strong interactions between the ZnO and PPy matrix were revealed by the widening of these bands in the composites. The improved thermal stability of the microcomposites was demonstrated by thermogravimetric analysis. The accelerated carrier separation across the large interface between ZnO and PPy, together with the rapid dissipation of electrons, reduces the carrier recombination in the PPy effectively, thereby enhancing its photocatalytic property for PPy-ZnO microcomposites. The abundance of active sites is contingent upon surface area, while the recombination processes of electron-hole pairs are regulated by band gap energy. Among the microcomposites, PPy-2% ZnO displays a larger band gap energy than PPy-5% ZnO and a greater surface area compared to PPy-1% ZnO. Consequently, it boasts more active sites than PPy-1% ZnO and, simultaneously, mitigates recombination reactions more effectively than PPy-5% ZnO. These attributes collectively contribute to a heightened degree of photocatalytic reactions.

Categories: Catalysis and Reaction Engineering, Materials Engineering, Nano Materials
Keywords: polymer microcomposite, photocatalyst, water remediation, band-gap, rhodamine 6g

Introduction

Macromolecules such as conducting polymers have been extensively studied due to their chemical stability in electrolytic solutions, ease of synthesis, low production cost, environmental safety, high thermal stability, and non-toxic nature [1-3].

The optical, electrical, and optoelectronic properties of polymer-inorganic composites can be enhanced compared to those of the individual components by blending organic polymers with inorganic compounds [4-8].

Polypyrrole (PPy) stands out as one of the most extensively studied conducting polymers due to its attractive properties, including relatively robust environmental stability, affordability, high conductivity, and ease of preparation [9,10]. It has been used in diverse fields such as sensors, actuators, electrodes, electrochemical capacitors, rechargeable batteries, corrosion-resistant coatings, electrochromic devices, varistors, fuel cell electrodes, and supercapacitors. As zinc oxide (ZnO) is a multi-functional inorganic material bearing properties such as high oxidation activity, good transparency, high electron mobility, thermal stability, and photosensitivity, it has emerged as an important material for potential applications in many research areas [11-14].

The conventional photocatalyst ZnO has been widely studied due to its great photocatalytic activity. ZnO may be significantly enhanced in its photocatalytic capabilities by combining it with other materials, such as polymers and inorganic and organic molecules. This synergistic combination creates a more effective photocatalytic reaction by using the unique properties of each substance. ZnO may be combined with these materials to significantly increase its overall activity, which makes it more useful for the photocatalytic reactions [15,16]. Polymer materials in the form of nano/microcomposites are useful due to certain advantages such as a high surface area-to-volume ratio [15-17].

The photocatalytic uses of PPy in water remediation processes, organic pollutants, and effluents have proven successful due to its large surface area, redox ability, adjustable band gap, π-electron conjugate

system, and electron-hole mobility. However, the functionality of PPy is reduced due to its limited adsorption capacity, recombination processes, and tendency to aggregate through π-π interactions. Blending of semiconductors with the conductive network is an operational way to reduce backward recombination and speeding up the charge transfer [18]. Conducting polymers, when used as photosensitizers, donate photon-induced electrons to ZnO. This process preserves the holes, reducing backward recombination and resulting in enhanced photocatalytic activity. [17,19]. Thus, PPy in good contact with ZnO at varying concentrations would exhibit high photocatalytic performance.

In the present work, the synthesis and modification of PPy to PPy-ZnO (PZ) microcomposites through in situ polymerization in the presence of ZnO microspheres (MSs) have been carried out. Different concentrations of ZnO are used for tuning the threshold efficiency of the composites for photocatalytic applications in dye degradation. A plausible mechanism for the PZ (p-n type) photocatalysis is discussed.

Materials And Methods

Materials

All chemicals such as zinc acetate dihydrate and *N*-cetyl-*N*,*N*,*N*-trimethyl ammonium bromide were acquired from Loba Chemie Pvt. Ltd. (India). Dioctyl sulfosuccinate sodium salt (Aerosol-OT, 96%) was purchased from Acros (Belgium). Ammonium persulfate and diethylene glycol (DEG) were procured from Fisher Scientific (India) and SD Fine Chem. Ltd. (India). Pyrrole (98%) was acquired from Sisco Research Laboratories Pvt. Ltd. (India). Ethanol used was of commercial grade. Pyrrole monomer was purified before use and stored in the dark at low temperatures. Deionized (DI) water was used throughout the synthesis.

Synthesis of ZnO MSs by polyol method

ZnO spheres were synthesized through the hydrolysis of zinc acetate in DEG. To a solution of 2.195 g of Zn(ac)2·2H_2O and 4 mM of *N*-cetyl-*N*,*N*,*N*-trimethyl ammonium bromide in 100 ml of diethylene glycol, vigorous stirring was applied for 15 min to ensure uniformity. The resulting mixture was then refluxed at 160°C for 12 h in a silicon oil bath fitted with a heating coil and dimmerstat. Following this, the ZnO precipitate was isolated via centrifugation, and the particles were thoroughly washed with ethanol. The obtained ZnO powder was subsequently dried in an oven and further subjected to calcination at 400°C for 3 h.

Synthesis of PPy by chemical oxidative polymerization method

Chemical oxidative polymerization method was adopted for the synthesis of PPy. Approximately 0.1 M pyrrole monomer and dioctyl sulfosuccinate sodium salt (AOT) were dissolved in 100 ml ethanol in a round-bottom flask and stirred with a magnetic stirrer to obtain a homogenous solution. On the other hand, 0.3 M ammonium persulfate (APS) was dissolved in 100 ml water and added dropwise with the help of a Soxhlet funnel to ethanol kept under constant stirring at room temperature. As the addition of APS in ethanol progressed, the colour of the solution gradually changed from colourless to black with precipitation. After complete addition of APS, the solution mixture was kept under constant stirring (1,200 rpm) for further 24 h at room temperature for completion of polymerization reaction (Scheme 1, Route I). The precipitate thus formed was collected and filtered through Whatman No. 41, followed by washing with ethanol and finally with distilled water several times to remove excess ions and unreacted monomer. The polymer was dried in an oven at 45°C.

Synthesis of PZ microcomposites

PZ microcomposites were synthesized via in-situ polymerization. Approximately, 0.1 M pyrrole monomer was dissolved in 100 ml ethanol. The desired wt.% of ZnO MSs was added to the monomer solution and stirred for 30 min to obtain a suspension (Scheme 1, Route II). Approximately, 0.3 M APS was dissolved in 100 ml of DI water and added dropwise to pyrrole-ZnO solution through a Soxhlet at a room temperature. The darkening of the solution indicated the formation of the polymer, and the reaction mixture was stirred for up to 24 h. After the completion of polymerization, the black-coloured precipitate was collected and washed with ethanol and DI water. Further, it was dried in an oven at 45°C to obtain PZ microcomposite powder.

Results

Different sophisticated analytical methods were employed to characterize all the synthesized samples. Fourier transform infrared (FTIR) spectra were recorded on Tensor 37 (Bruker, USA) over the range of 4,000-400 cm^{-1} at room temperature. Crystallinity of samples was determined using X-ray diffraction (XRD) technique with a Rigaku Ultima-IV powder X-ray diffractometer with CuKβ radiations (λ = 1.5406 Å). Field emission scanning electron microscopy (FESEM) analysis using a Quanta FEG-450 was employed to obtain the morphology of the samples. Energy-dispersive X-ray (EDX) spectroscopy, equipped along with FESEM, was used to record the elemental composition and mapping images of all samples. The

Thermo Fisher Scientific SURFER instrument was used for the measurement of specific surface area (using the Brunauer-Emmett-Teller [BET] method) and pore diameter (using the Barrett-Joyner-Halenda method). Raman spectroscopy was used to investigate the surface and interfacial interactions between PPy and ZnO using laser light 532 nm as an excitation source under ambient conditions. Thermal stability of all the sample was studied using Perkin Elmer STA6000 instrument. The absorption edge and band gap of bare and composites were calculated using ultraviolet-visible (UV-Vis) spectra recorded on a UV-Vis spectrophotometer (Shimadzu, Japan) within the range 200 to 800 nm.

Discussion

XRD study

Figure *1* displays the XRD patterns of ZnO, PPy, and PPy-ZnO composites with varying weight percentages of ZnO (1, 2, and 5). The XRD pattern of ZnO exhibits prominent peaks at 2θ = 31.70, 34.49, and 36.14, confirming the microcrystalline hexagonal wurtzite crystal structure (with lattice parameters a = 3.2555 Å and c = 5.1935 Å), consistent with the data from the JCPDS card no. 36-1451 [20]. The absence of additional peaks indicates the formation of a pure phase of ZnO MSs [21].

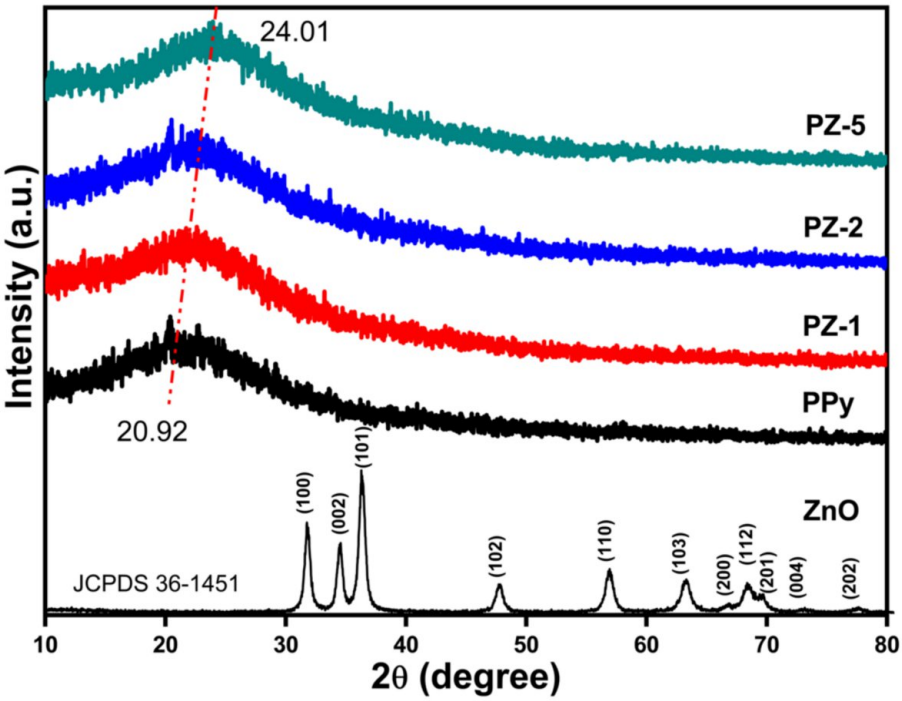

FIGURE 1: ZnO and PPy-ZnO microcomposites with varied ZnO (1, 2, and 5 wt.%) concentrations were examined with an X-ray diffraction pattern.

PPy: polypyrrole, ZnO: zinc oxide, PZ: polypyrrole-zinc oxide

In the XRD pattern of PPy, a broad peak centered ~2θ = 20.92 can be attributed to the repeat unit of the pyrrole ring, suggesting high orientation of the polymer chain [20]. The broadening of this peak indicates the amorphous nature of the polymer. As the percentage of ZnO MSs grows from 1 to 5 wt.% in the PPy-ZnO composites, the wide peak moves towards higher 2θ angles, from 20.92 to 24.01. This shift may result from intermolecular interactions between the polypyrrole chains and ZnO MSs. On the other hand, the low concentrations may be the reason for the lack of identifiable peaks corresponding to ZnO MSs in the composites [22].

FTIR analysis

FTIR spectroscopy served to explore the structural properties of the materials. In Figure *2*, the FTIR spectra of ZnO, PPy, and their composites are presented. ZnO MSs exhibit characteristic bands at 480, 557, and 3,412 cm^{-1} in their spectra. The stretching vibration modes of the Zn-O bond manifest at 480 and 559 cm^{-1}. The broad band observed at 3,428 cm^{-1} likely arises from moisture adsorbed onto the oxide's surface [23]. In the FTIR spectra of PPy and PPy-ZnO composites, bands appear at 3,220, 2,960, 1,704, 1,604,

1,208, 1,040, 794, and 586 cm^{-1}. The wide band at around 3,220 cm^{-1} corresponds to the N-H stretching vibrations, while the peak at 586 cm^{-1} represents the N-H in-plane deformation of the PPy ring. The band at 2,960 cm^{-1} is attributed to the symmetric stretching of the -CH_2 groups. The stretching vibrations of the PPy ring's C=C and C-C bonds are observed at 1,704 and 1,604 cm^{-1}, respectively. Additionally, the bands at 1,208, 1,040, and 794 cm^{-1} correspond to the stretching vibrations of the C-H and C-N bonds, as well as the out-of-plane ring deformations [24,25].

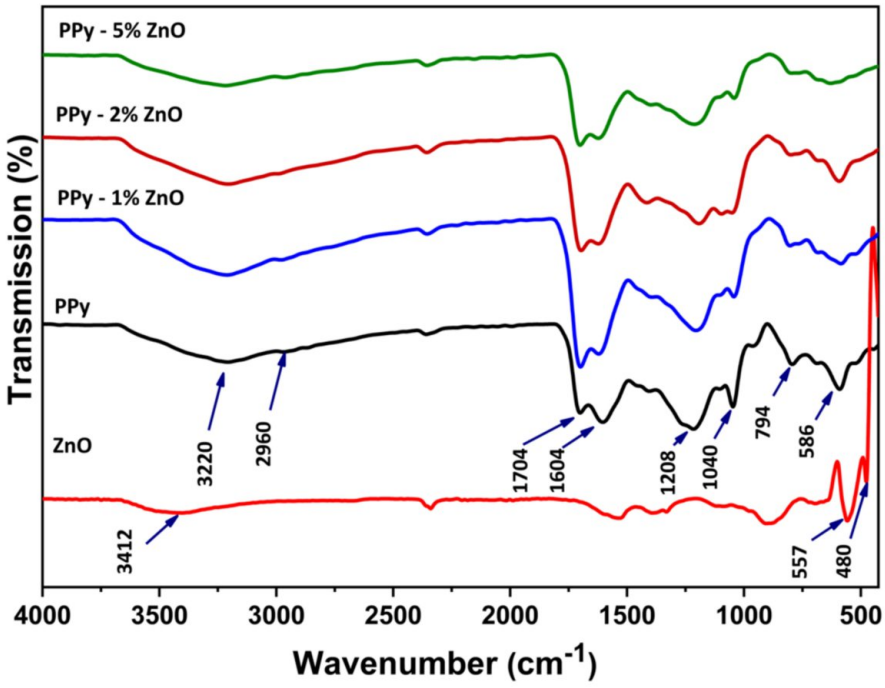

FIGURE 2: FTIR spectra of ZnO, PPy, and PPy-ZnO microcomposites.

FTIR: Fourier-transform infrared, ZnO: zinc oxide, PPy: polypyrrole

The band in the PPy FTIR spectra that emerges at 586 cm^{-1} in PPy-ZnO (1, 2, and 5 wt.%) is shown to be extended, indicating that strong interactions between PPy and ZnO MSs persist and lead to a change in polymer conformation [26].

Raman analysis

Raman analysis was utilized to explore the intermolecular interactions between ZnO microstructures (MSs) and the PPy chain. In Figure *3*, the Raman spectra of ZnO, PPy, and PPy-ZnO composites are depicted within the frequency range of 600 to 1800 cm^{-1}. Distinctive Raman bands are evident in the ZnO spectra, appearing around 328, 438, and 586 cm^{-1} (Figure *3a*). Notably, a second-order Raman band emerges near 328 cm^{-1}. The pronounced, high-intensity sharp band (E2H) at approximately 438 cm^{-1} signifies the characteristic hexagonal wurtzite structure of ZnO, indicating its excellent crystallinity. Moreover, the band observed at 586 cm^{-1} is linked to oxygen vacancies within ZnO [27]. In the Raman spectrum of PPy (Figure *3b*), the ring stretching mode of the polymer backbone and its π conjugated structure manifest as peaks at approximately 1,570 and 1,323 cm^{-1}, respectively. The presence of the quinoid polaronic and bipolaronic structure is indicated by a minor peak at 934 cm^{-1}, while the peak at 1,045 cm^{-1} corresponds to the C-H in-plane deformation [26,28].

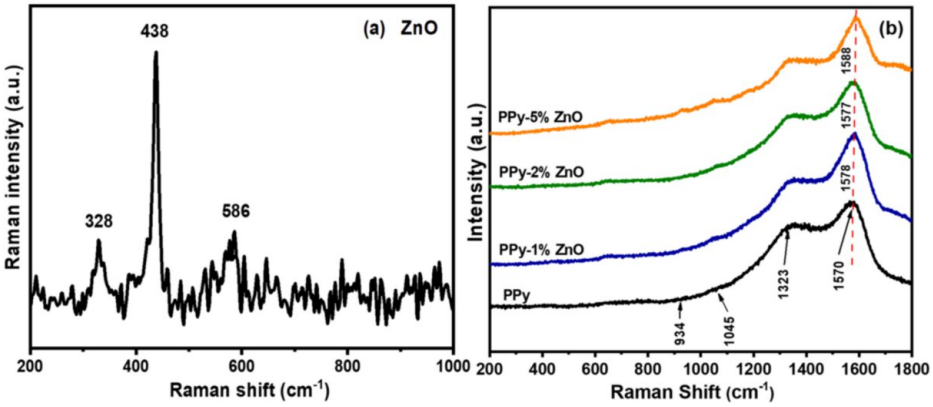

FIGURE 3: Raman spectra of (a) ZnO and (b) PPy and PPy-ZnO (1, 2, and 5 wt.%) microcomposites.

ZnO: zinc oxide, PPy: polypyrrole

The peak in PPy that appears at 1,570 cm^{-1} is observed to be displaced to higher frequencies (1,578, 1,577, and 1,588 cm^{-1}) in microcomposites that include 1, 2, and 5 wt.% of ZnO, respectively. This shift confirms that ZnO is encapsulated in the PPy matrix and is ascribed to the conjugational interactions between ZnO and PPy [29].

Studies of optical properties

The UV-Vis absorption spectra of PPy and PPy-ZnO microcomposites with varied concentrations of ZnO are depicted in Figure *4*. ZnO, as a semiconductor, exhibits a band edge at 354 nm, while PPy shows a band edge at 651 nm attributed to π-π* electronic transitions [30]. With an increase in ZnO content within the microcomposites, a band edge emerges between the two materials, shifting towards longer wavelengths. Notably, even minute concentrations (1, 2, and 5 wt.%) of ZnO induce a noticeable shift in wavelength from 651 to 490 nm, as depicted in Figure *4*.

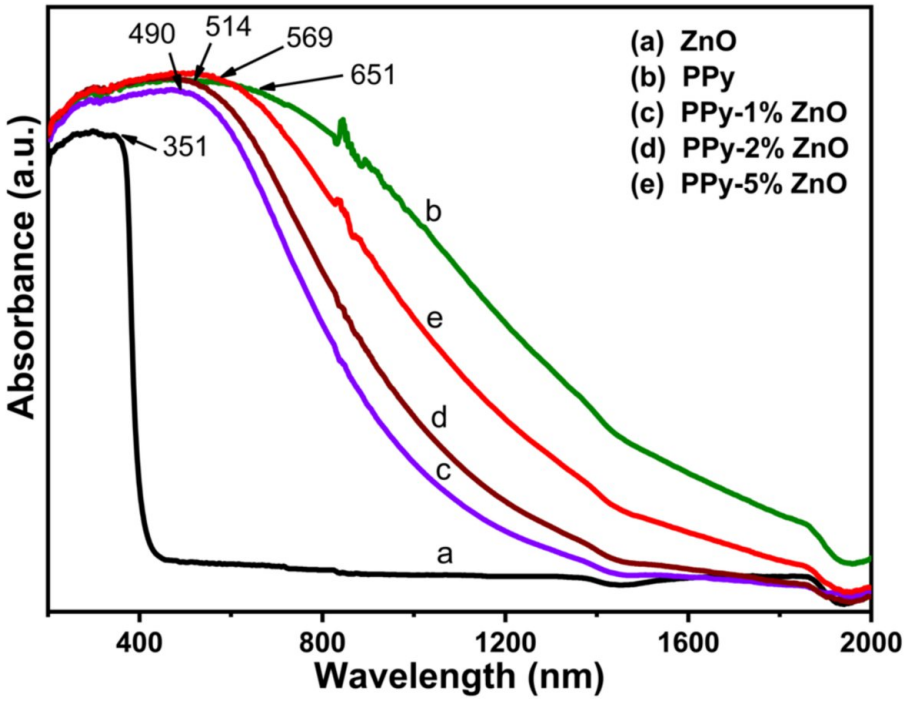

FIGURE 4: Ultraviolet-visible absorption spectra of ZnO, PPy, and PPy-ZnO (1, 2, and 5 wt.%) microcomposites.

ZnO: zinc oxide, PPy: polypyrrole

The reason for this may be the effortless transfer of p electrons from PPy to the electronic bands of ZnO, which suggests strong interactions between the two. From the Tauc's plot (Figure *5*), the optical band gaps of ZnO, PPy, and PPy-ZnO (1, 2, and 5 wt.%) microcompites have been determined using Equation (1):

$$(\alpha h\nu)^2 = A(h\nu - Eg) \quad (1)$$

where A is a constant, α is the optical absorption coefficient, hν is the photon energy, and Eg is the optical band gap. The calculated band gap energy values are given in Table *1*.

Sr. No.	Sample	Absorption band (nm)	Band gap (eV)
1	ZnO	351	3.16
2	PPy	651	0.92
3	PPy-1% ZnO	490	1.44
4	PPy-2% ZnO	514	1.33
5	PPy-5% ZnO	569	1.12

TABLE 1: Absorbance edges and band gap energies for ZnO, PPy, and PPy-ZnO microcomposites

ZnO: zinc oxide, PPy: polypyrrole

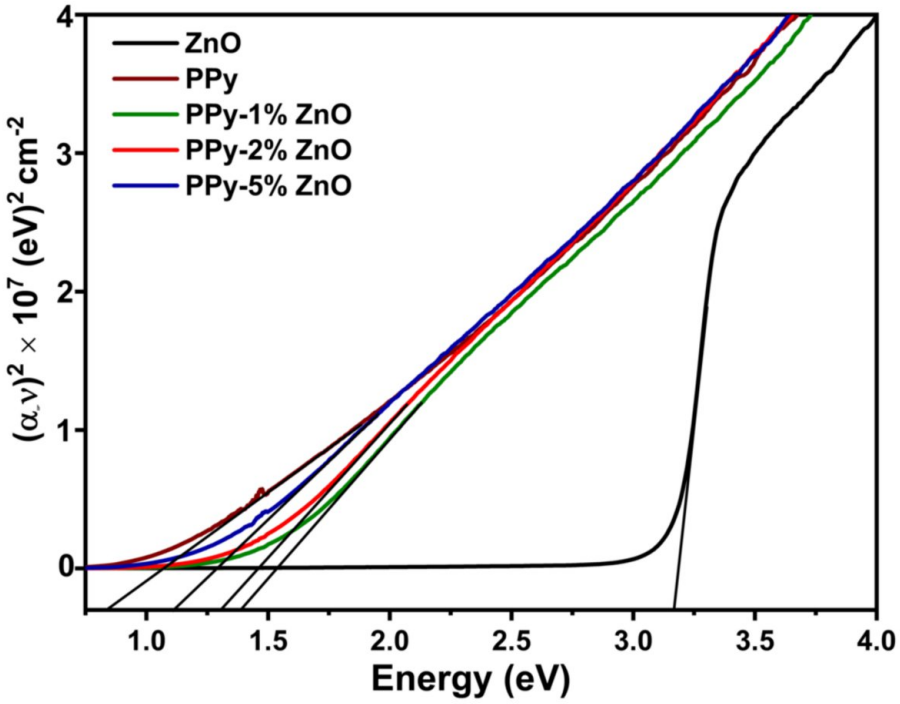

FIGURE 5: Optical band gap for ZnO, PPy, and PPy-ZnO (1, 2, and 5 wt.%) microcomposites.

ZnO: zinc oxide, PPy: polypyrrole

ZnO and PPy have optical band gaps of 3.16 and 0.92 eV, respectively, as noted from Table *1*. In contrast, for composites, it is observed that the band gap rises with the weight percentage of ZnO relative to PPy. This demonstrates unequivocally that ZnO is important and influences the interfacial properties of PPy-ZnO composites.

Morphological and compositional analysis

Morphological tuning is a useful technique for directing the characteristic properties of material and capabilities in a variety of application domains. The physical and chemical qualities of materials are determined by their surface and morphological modification, which ultimately determines their suitability and practicality. Therefore, it becomes essential to comprehend particle form and behavior. The surface morphologies of ZnO, PPy, PPy-1% ZnO, PPy-2% ZnO, and PPy-5% ZnO composites are displayed in Figure *6a*-e, respectively.

As seen in Figure *6*, PPy and pure ZnO MSs exhibit a semi-uniform spherical shape, which is superior than that seen in the previous literature [24,31-32]. The ZnO micrographs were observed with the size varying between 0.2 and 0.6 μm and the average particle size of 0.4 μm (Figure *6a*).

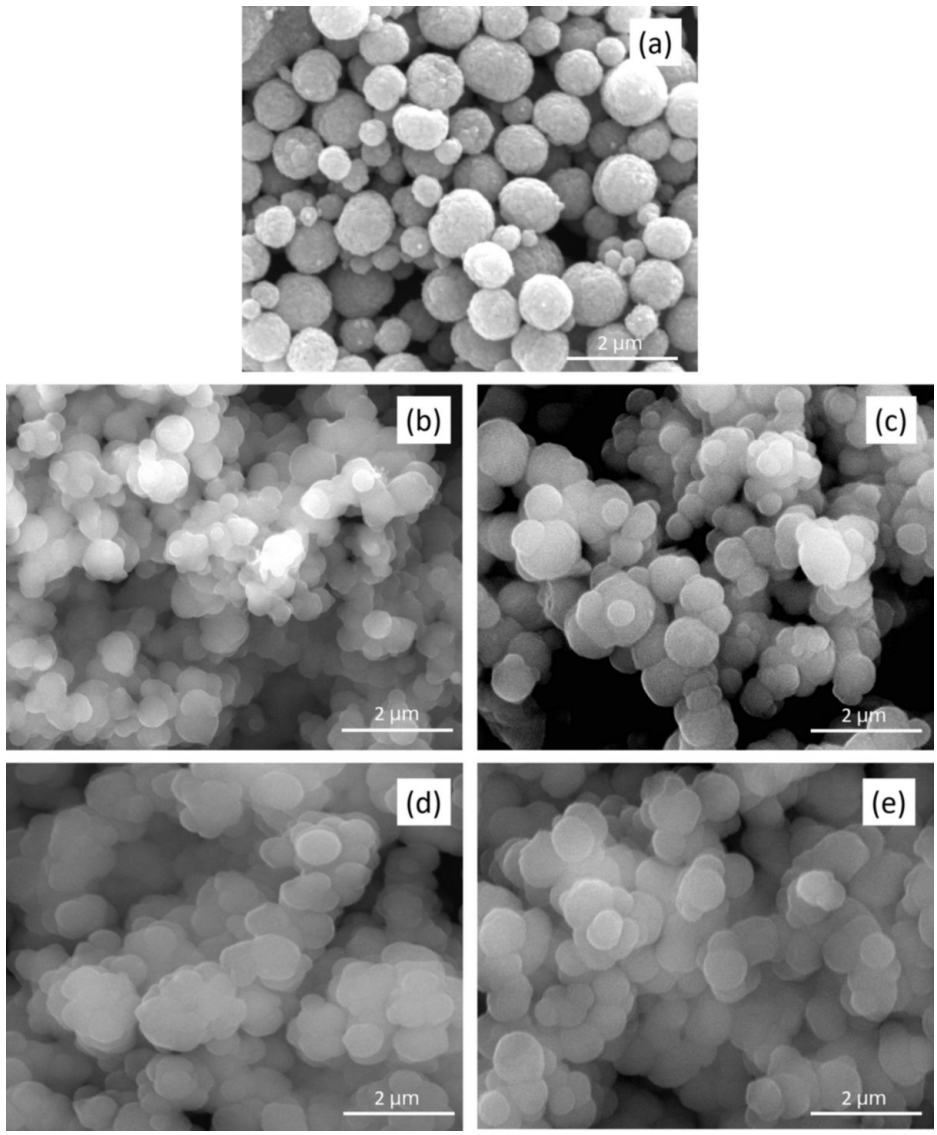

FIGURE 6: FESEM micrographs of (a) ZnO, (b) PPy, and (c-e) PPy-1% ZnO, PPy-2% ZnO, and PPy-5% ZnO microcomposites.

ZnO: zinc oxide, PPy: polypyrrole, FESEM: field emission scanning electron microscopy

The FESEM micrographs of the original PPy and the PPy-1% ZnO, PPy-2% ZnO, and PPy-5% ZnO composites are exhibited in Figure *6b*-e, respectively. An increase in the weight percentage of ZnO is noticed in the compactness between the particles. This suggests that there are more robust interactions between ZnO and PPy. Table *2* provides the distribution of particle sizes as well as the average particle size.

Sr. No.	Sample	Average particle size (μm)	Particle size distribution (μm)
1	PPy-1% ZnO	0.43	0.2-0.75
2	PPy-2% ZnO	0.34	0.2-0.45
3	PPy-5% ZnO	0.32	0.2-0.41
4	ZnO	0.39	0.2-0.55
5	Polypyrrole	0.41	0.2-0.65

TABLE 2: Particle size distribution and the average particle size observed for ZnO, PPy, and PPy-ZnO microcomposites

ZnO: zinc oxide, PPy: polypyrrole

The table reveals that as the concentration of ZnO in the composites increases, there is a decrease in particle size distribution. This is probably because, when there are fewer ZnO particles present (1 wt.% ZnO) during polymerization, a larger amount of polymer tends to deposit onto each individual ZnO particle. However, at higher concentrations (2 and 5 wt.% ZnO), where a greater number of particles are present during polymerization, the amount of polymer surrounding each particle diminishes, resulting in a decrease in the average particle size distribution [20].

EDX analysis

The elemental mapping images (EDX) of PPy-1% ZnO, PPy-2% ZnO, and PPy-5% ZnO microcomposite are shown in Figure 7. The presence of C, N, Zn, and O can be seen from the EDX images. The elemental compositions of the PPy-ZnO composites are given in Table 3.

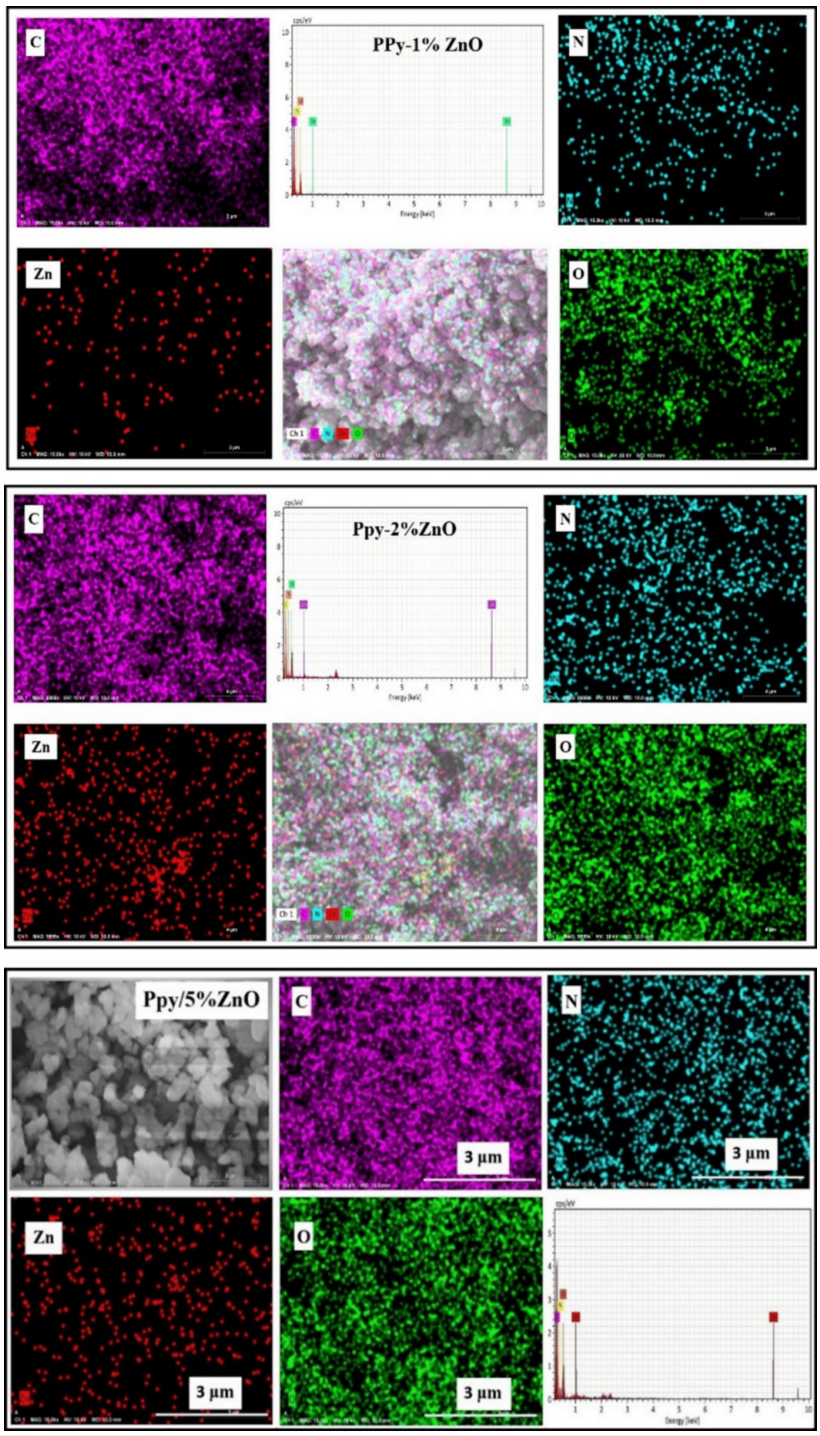

FIGURE 7: The elemental mapping images of PPy-ZnO (1, 2, and 5 wt.%) microcomposites.

ZnO: zinc oxide, PPy: polypyrrole

Sr. No.	Composites	Atom (wt.%)			
		Zn	O	N	C
1	PPy-1% ZnO	0.45	36.19	10.08	53.28
2	PPy-2% ZnO	0.86	29.19	11.18	58.77
3	PPy-5% ZnO	1.4	36.08	12.07	50.45

TABLE 3: Elemental compositions obtained for PPy-ZnO (1, 2, and 5 wt.%) composites from EDX analysis

ZnO: zinc oxide, PPy: polypyrrole, EDX: energy-dispersive X-ray spectroscopy, C: carbon, N: nitrogen, Zn: zinc, O: oxygen

Thermogravimetric analysis

Thermogravimetric analysis was used to elucidate the thermal behaviour of PPy and composites containing varying weight percentages of ZnO (1, 2, and 5 wt.%) in an N_2 environment. The thermograms of all the samples are shown in Figure *8*. Except ZnO, all thermograms depict the minor initial weight loss of around 10-12% between room temperature and 100°C, followed by a two-step fast loss that occurs between 100°C and 750°C.

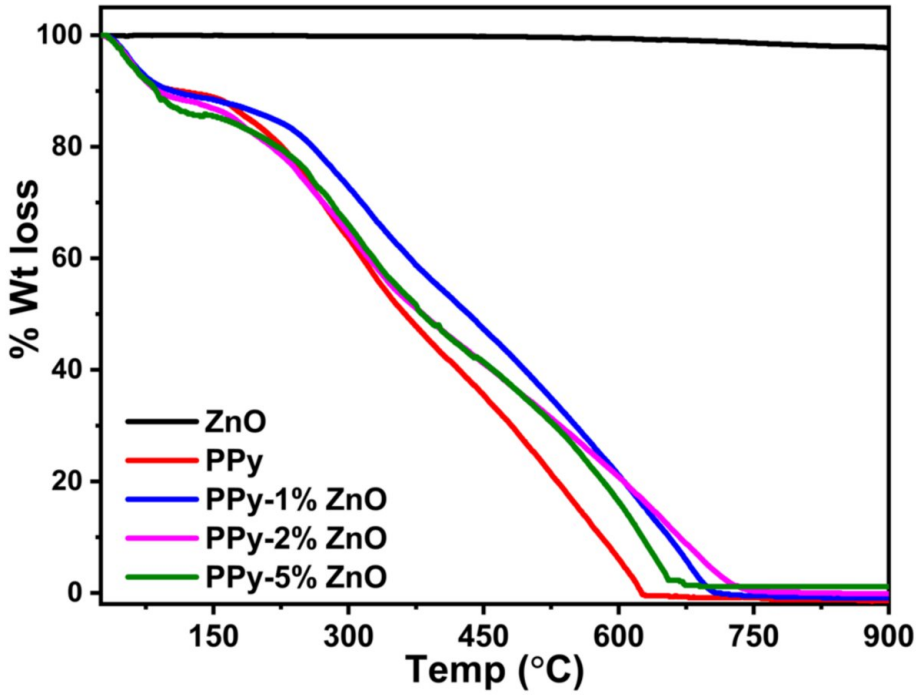

FIGURE 8: TGA curves of ZnO, PPy, and PPy-ZnO (1, 2, and 5 wt.%) microcomposites in N2 atmosphere.

ZnO: zinc oxide, PPy: polypyrrole, TGA: thermogravimetric analysis

The evacuation of moisture that had been adsorbed on the surface of samples is responsible for the initial little weight loss. The fast weight loss in the next phases is caused by the loss of dopant ions, the thermal oxidative breakdown of smaller polymer fragments, and, in the case of composites, the full degradation of PPy with very little residue [33]. The high thermal stability of ZnO and strong interactions between PPy and ZnO can lead to an improvement in thermal stability and a shift in the decomposition temperature of composites. Indeed, ZnO is a stable oxide, and weight loss is expected to be limited to traces of adsorbed water molecules.

Surface area analysis (BET)

As observed from Table 4, ZnO has the lowest surface area, and PPy has the greatest surface area. When it comes to composites, the surface area of the PPy/1 wt.% ZnO composite is even smaller at 6 $m^2 g^{-1}$ than that of ZnO (8 $m^2 g^{-1}$), and it further shows increases at 2 and 5 wt.% of ZnO, respectively.

These findings suggest that despite being present in small concentrations within the composites, the surface area is primarily influenced by ZnO. This conclusion finds support in the FESEM analysis, which illustrates a reduction in particle size corresponding to the increase in wt.% of added ZnO.

Sample	PPy	ZnO	PPy-1% ZnO	PPy-2% ZnO	PPy-5% ZnO
Surface area (m^2/g)	14	8	6	9	10

TABLE 4: Specific surface area of pristine ZnO, PPy, and PPy-ZnO composites (1, 2, and 5 wt.%)

ZnO: zinc oxide, PPy: polypyrrole

Photocatalytic activity of pure PPy, ZnO, and PPy-ZnO microcomposites

The activity of ZnO as a catalyst is dependent on specific wavelengths of light, often in the UV range. This is because ZnO has a wide band gap (~3.16 eV) that requires UV light to generate electron-hole pairs necessary for the photocatalytic reactions. Hence, photocatalytic degradation of R6G was performed under UV light source (UVA, 320-400 nm, Philips) in the presence of ZnO, PPy, and PPy-ZnO (1, 2, and 5 wt.%) microcomposites. The aqueous suspension of R6G was prepared by adding 30 mg of pure PPy photocatalyst into optimized 2.5 × 10^{-5} M R6G solution. UV light irradiation was carried out in a quartz cell attached with a cooling jacket to avoid the thermal degradation. At known time intervals, the decomposed dye aliquot was withdrawn, followed by centrifugation. The decreased concentration of R6G was measured in terms of absorbance at 526 nm using a UV spectrophotometer. The photodegradation efficiency of the composites was calculated according to Equation (2):

$$\text{Degradation efficiency} = \frac{C_0 - C_t}{C_t} \times 100 \quad (2)$$

where C_0 and C_t are the concentrations of dye at initial time and at time ‘t’, respectively.

The photocatalytic degradation of an aqueous solution of organic dye is a first-order reaction, and its rate constant was calculated by Equation (3), as follows:

$$C = C_0 \times e^{-kt} \quad (3)$$

where k is the rate constant, and C0 and C are the initial concentration and concentration at the reaction time ‘t’, respectively.

The possible photocatalytic reaction mechanism is illustrated in Figure 9.

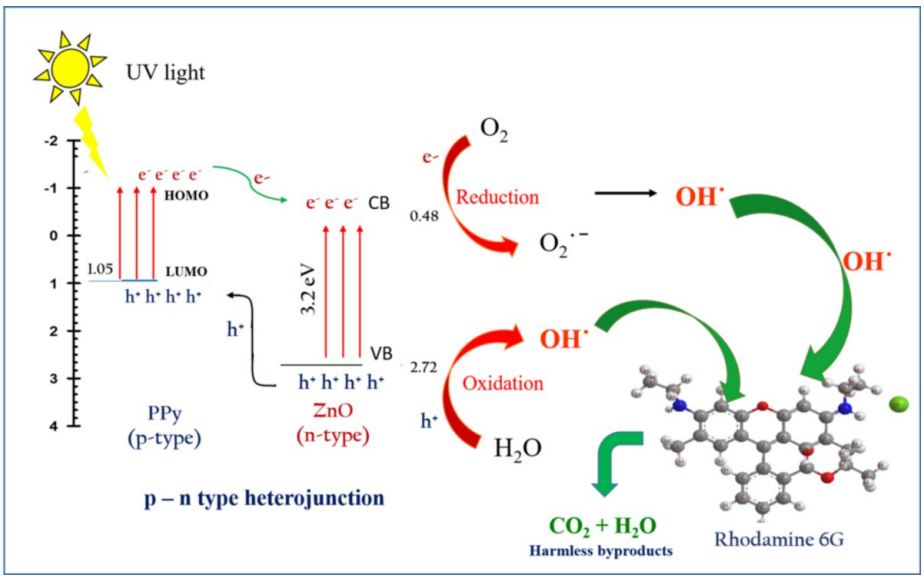

FIGURE 9: Schematic representation of carrier separation and transport mechanism at the PPy-ZnO interface.

ZnO: zinc oxide, PPy: polypyrrole

The photocatalytic mechanism of p-n type PPy-ZnO microcomposite is shown in Scheme 2, and conversion reactions are as follows:

$$ZnO + h\nu \rightarrow ZnOe_{cb}^{-} + ZnOe_{vb}^{+}$$

$$PPy + h\nu \rightarrow PPye_{cb}^{-} + PPye_{vb}^{+}$$

$$ZnOe_{vb}^{+} \overset{Transform}{\rightarrow} PPye_{vb}^{+} \rightarrow ZnOe_{vb}^{+} + PPye_{vb}^{+} \text{ (hole carrier)}$$

$$PPye_{cb}^{-} \overset{Transform}{\rightarrow} ZnOe_{cb}^{-} \rightarrow ZnOe_{cb}^{-} + PPye_{cb}^{-} \text{ (electron carrier)}$$

$$e_{cb}^{-} + O_2 \rightarrow O_2^{\cdot -} \text{ (electron trapping)}$$

$$H_2O \rightarrow H^{+} + OH^{-}$$

$$O_2^{\cdot -} + H^{+} \rightarrow {}^{\cdot}OOH$$

$${}^{\cdot}OOH + H^{+} + e_{cb}^{-} \rightarrow H_2O_2$$

$$H_2O_2 + e_{cb}^{-} \rightarrow {}^{\cdot}OH + OH^{-}$$

$$h_{vb}^{+} + H_2O \rightarrow H^{+} + OH^{-}$$

$$h_{vb}^{+} + OH^{-} \rightarrow {}^{\cdot}OH$$

$${}^{\cdot}OH + R6G \rightarrow CO_2 + H_2O \text{ (degraded products)}$$

ZnO absorbs UV light of a wavelength below 400 nm due to a wide band gap and is mostly transparent to visible light, while PPy absorbs light in the visible region due to short band gap. Photocatalytic dye degradation ability of ZnO, PPy, and PPy-ZnO (1, 2, and 5 wt.%) microcomposites with respect to time is shown in Figure *10*, and its rate constants are given in Table *5*.

Sr. No.	Photocatalyst	Time required for degradation (min)	Photocatalytic degradation (%)	Rate constant (k) (min^{-1})
1	ZnO	180	68.68	2.326×10^{-2}
2	PPy	180	49.82	1.524×10^{-2}
3	PPy-1% ZnO	06	93.04	7.446×10^{-2}
4	PPy-2% ZnO	06	98.19	3.035×10^{-1}
5	PPy-5% ZnO	13	80.34	2.090×10^{-3}

TABLE 5: Photocatalytic degradation capability and the rate constants of ZnO, PPy, and PPy-ZnO microcomposites

ZnO: zinc oxide, PPy: polypyrrole

PPy with a much smaller band gap cannot generate carriers effectively under UV light. As a result, photogenerated electrons and holes recombine rapidly. This was confirmed by demonstrating the very low photocatalytic activity by PPy up to only 49.82% in 180 min. Pure ZnO shows 68.68% catalytic activity. The combination of PPy and ZnO MSs at 1, 2, and 5 wt.% concentration attained a more significant photocatalytic property than either material alone owing to the highly reduced recombination ratio [34]. The rate of degradation in a photocatalytic reaction is usually faster at the start and slows down over time due to several factors. Initially (for the first minute), the high concentration of reactants undergoes rapid interactions with the photocatalyst, resulting in degradation. As time progresses, the concentration of reactants, as well as the number of active sites on the catalyst, decreases, leading to slowing down of the reaction. Additionally, active sites on the photocatalyst's surface may be blocked by intermediate products, reducing their availability. There is no catalyst poisoning during the degradation process. Intermediate products also compete with original reactants for active sites, further decreasing the rate. Finally, light absorption efficiency decreases as intermediates form and solution properties change, such as increased turbidity, which scatters or blocks light, resulting in a decrease in the degradation rate.

As observed from Figure *10* and Table *5*, the amount of dye degraded in the presence of ZnO is ~68.68%. Among all the microcomposites, PPy-2% ZnO shows the highest photocatalytic activity with 98.19% degradation of dye in only 6 min, while PPy-1% ZnO and PPy-5% ZnO exhibit 93.04% and 73.51% degradation, respectively, in the presence of UV light. The photocatalytic property of PZ-2 sample is observed to be enhanced by more than ~25% compared to bare ZnO and other composites [35]. PPy-2% ZnO composite show high rate constant as it exhibits the highest photocatalytic activity.

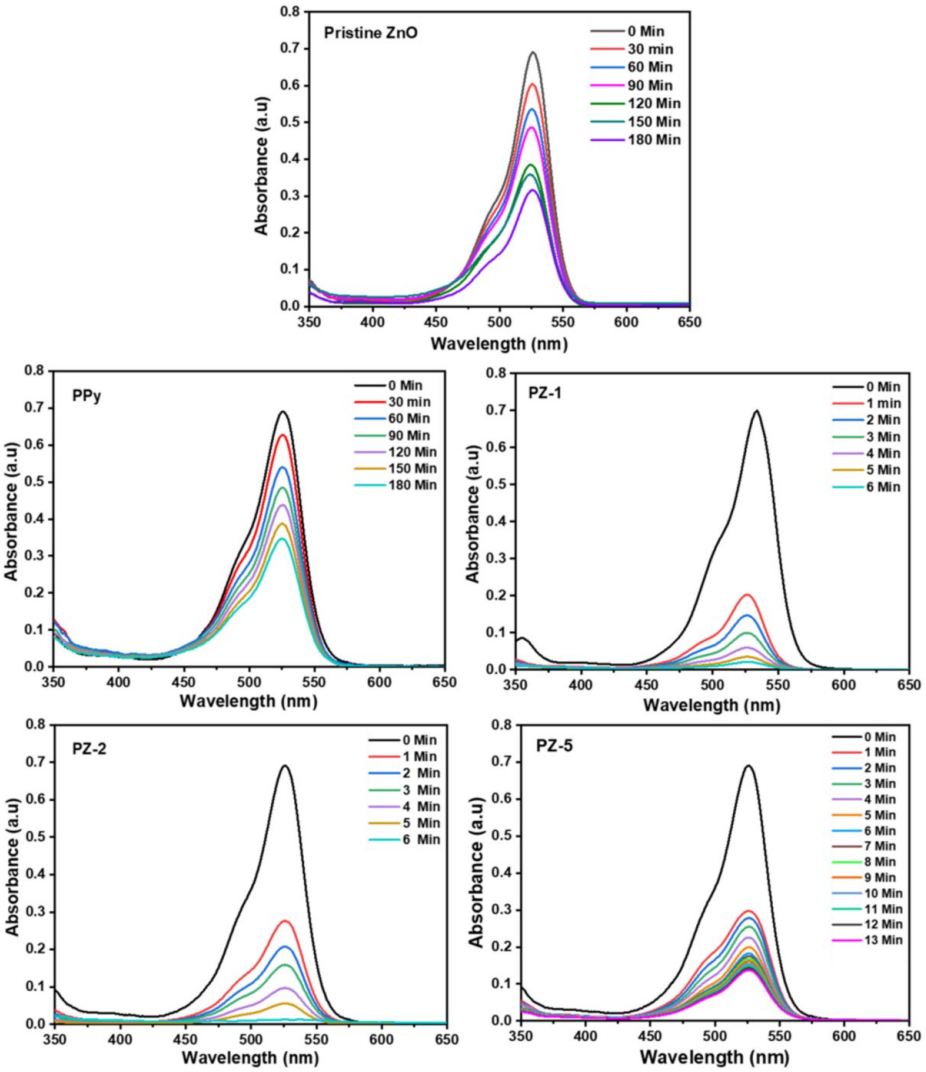

FIGURE 10: Photocatalytic degradation of rhodamine 6G as a function of time in the presence of ZnO, PPy, and PPy-ZnO (1, 2, and 5 wt.%) microcomposites under the UV light irradiation.

ZnO: zinc oxide, PPy: polypyrrole, UV: ultraviolet

Although these results are contrary to the specific surface area, the results are governed by the density of ZnO present in the microcomposites [36]. These results can be explained on the basis of surface area and band gap energies of the samples, which appear to be the competing factors in the photocatalytic reactions. The surface area contributes to the number of active sites, while band gap energy controls the electron-hole pair recombination reactions. As observed from the results, PPy-2% ZnO has band gap energy higher than PPy-5% ZnO and higher surface area compared to PPy-1% ZnO. Hence, it bears higher number of active sites compared to PPy-1% ZnO, and, at the same time, it efficiently reduces the degree of recombination reactions compared to PPy-5% ZnO, both the factors contributing towards higher degree of photocatalytic reactions [37].

The lack of a consistent trend in the degradation percentage with 1%, 2%, and 5% ZnO loading could be due to several factors. As seen from the results, the addition of just 1% of catalyst leads to an increase of more than 20% in degradation compared to pristine ZnO, and the degradation is almost 98% in the presence of 2% catalyst, which is close to 100%. Further addition of 5% does not show an increase in degradation since a negligible amount of dye molecules are left in the solution. In fact, it leads to a decrease in the percent degradation, which might be due to particle agglomeration and light scattering, thereby reducing the effective light absorption ability. Also, higher concentration of catalyst may promote an increase in the recombination rate of photogenerated electron-hole pairs, which lowers the photocatalytic efficiency. These combined effects result in non-linear and inconsistent degradation percentage at higher loading levels of ZnO.

After collecting the catalyst from the reaction mixture, it was submerged in a solvent and then sonicated to evaluate whether the dye could be adsorbed or absorbed onto the photocatalyst. The absence of dye separation from the catalyst is noteworthy as it suggests that the dye molecules were not adsorbed or absorbed onto the catalyst surface [38]. This finding highlights the photocatalyst's effectiveness in promoting the breakdown of dye pollutants without enduring major interactions that could compromise its catalytic activity.

Reusability study of microcomposites

The reusability of PZ photocatalysts (with 1 wt.%, 2 wt.%, and 5 wt.% ZnO) was assessed under consistent conditions. After the first cycle of photocatalytic reactions with R6G in an aqueous solution, the photocatalysts were carefully collected. Following a simple washing and drying process, these photocatalysts were reused for additional three cycles under similar conditions. As shown in Figure *11*, in the case of PZ-1 and PZ-5, dye degradation decreased by 2-4% in subsequent cycles, while it is only ~2% in the case of PZ-2 microcomposite.

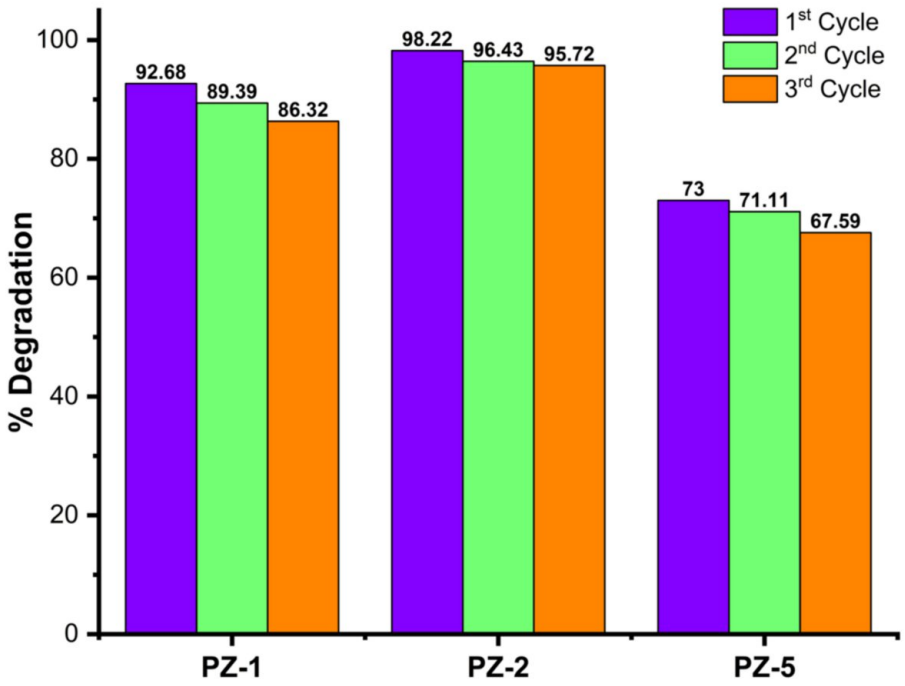

FIGURE 11: Percent degradation of R6G dye in three consecutive cycles in the presence of PZ nanocomposites.

R6G: rhodamine 6G, PZ: polypyrrole-zinc oxide

These results indicate that the PZ-2 photocatalyst retained higher efficiency in dye degradation process compared to PZ-1 and PZ-5 microcomposites. However, further work is needed to improve the process of recollection of catalyst after photocatalytic reactions.

Conclusions

Microcomposites comprising PPy-ZnO with low concentrations of ZnO (1, 2, and 5 wt.%) were successfully synthesized using chemical oxidative polymerization. In the FTIR spectrum of PPy-ZnO composites, distinct Zn-O and N-H stretching vibrations appeared at 480 and 3207 cm-1, indicating effective interlinking between PPy and ZnO. Introduction of ZnO MSs into the PPy matrix resulted in peak shifts in the XRD patterns, signifying intermolecular interactions between ZnO MSs and the PPy matrix. Morphological analysis revealed a compact spherical structure, with EDX analysis confirming the presence of C, N, Zn, and O elements, thus validating the incorporation of ZnO within the PPy matrix. Moreover, the thermal stability of PPy-ZnO composites surpassed that of pure PPy and exhibited a consistent increase with higher amounts of ZnO. UV-Vis spectra showed a shift in the band edge of PPy-ZnO composites towards higher wavelengths with an increase in ZnO wt.%, which is attributed to electron delocalization, supporting strong interactions between ZnO MSs and the PPy matrix. Among the PPy-ZnO microcomposites, enhanced photocatalytic performance stemmed from synergistic interactions. Accelerated separation of charge carriers across the extensive ZnO-PPy interface facilitated swift electron

transfer, minimizing carrier recombination within the PPy matrix and optimizing efficiency. Consequently, the photocatalytic property of PPy-2% ZnO significantly boosted up by more than ~25% compared to bare ZnO, and these results are found to be superior to previous reports.

Additional Information

Author Contributions

All authors have reviewed the final version to be published and agreed to be accountable for all aspects of the work.

Concept and design: Anjali A. Athawale

Critical review of the manuscript for important intellectual content: Anjali A. Athawale

Supervision: Anjali A. Athawale

Acquisition, analysis, or interpretation of data: Sudhakar B. Satpal

Drafting of the manuscript: Sudhakar B. Satpal

Disclosures

Human subjects: All authors have confirmed that this study did not involve human participants or tissue. **Animal subjects:** All authors have confirmed that this study did not involve animal subjects or tissue. **Conflicts of interest:** In compliance with the ICMJE uniform disclosure form, all authors declare the following: **Payment/services info:** All authors have declared that no financial support was received from any organization for the submitted work. **Financial relationships:** All authors have declared that they have no financial relationships at present or within the previous three years with any organizations that might have an interest in the submitted work. **Other relationships:** All authors have declared that there are no other relationships or activities that could appear to have influenced the submitted work.

Acknowledgements

The authors gratefully acknowledge Dr Babasaheb Ambedkar Research and Training Institute (BARTI), Government of Maharashtra, India, and Naval Research Board (417/MAT/18-19), Government of India, for the financial support. The authors express their sincere thanks to the Department of Chemistry, Savitribai Phule Pune University, Pune, for providing the infrastructural and characterization facilities during this work.

References

1. Sabouraud G, Sadki S, Brodie N: The mechanisms of pyrrole electropolymerization. Chemical Society Reviews. 2000, 29:283-293. 10.1039/a807124a
2. Nishio K, Fujimoto M, Ando O, Ono H, Murayama T: Characteristics of polypyrrole chemically synthesized by various oxidizing reagents. Journal of Applied Electrochemistry. 1996, 26:425-429. 10.1007/BF00251328
3. Wang J, Wu C, Wu P, Li X, Zhang M, Zhu J: Polypyrrole capacitance characteristics with different doping ions and thicknesses. Physical Chemistry Chemical Physics. 2017, 19:21165-21173. 10.1039/C7CP02707A
4. Chougule MA, Sen S, Patil VB: Facile and efficient route for preparation of polypyrrole-ZnO nanocomposites: Microstructural, optical, and charge transport properties. Journal of Applied Polymer Science. 2012, 125:E541-E547. 10.1002/app.36475
5. Gurbuz O, Senkal BF, Icelli O: Structural, optical and electrical properties of polypyrrole in an ionic liquid. Polymer Bulletin. 2017, 74:2625-2639. 10.1007/s00289-016-1856-3
6. De Oliveira HP, Andrade S, De Melo CP: Optical and dielectric properties of polypyrrole nanoparticles in a polyvinylalcohol matrix. Synthetic Metals. 2005, 155:631-634. 10.1016/j.synthmet.2005.08.017
7. Navale ST, Mane AT, Ghanwat AA, Mulik AR, Patil VB: Camphor sulfonic acid (CSA) doped polypyrrole (PPy) films: Measurement of microstructural and optoelectronic properties. Measurement. 2014, 50:363-369. 10.1016/j.measurement.2014.01.012
8. Kshirsagar K, Markad U, Saha A, Sharma K, Sharma G: Facile synthesis of palladium nanoparticles doped polyaniline nanowires in soft templates for catalytic applications. Materials Research Express. 2017, 4:025015. 10.1088/2053-1591/aa5947
9. Bhalerao AB, Bulakhe RN, Deshmukh PR, Jin J, Keshav S: Chemically synthesized 3D nanostructured polypyrrole electrode for high performance supercapacitor applications. Journal of Materials Science: Materials in Electronics. 2018, 29:15699-15707. 10.1007/s10854-018-9175-0
10. Huang J, Yang Z: Synthesis of ZnO/polypyrrole composites and an application in Zn/Ni rechargeable batteries. RSC Advances. 2014, 4:19205-19209. 10.1039/c4ra01322k
11. Huang J, Yin Z, Zheng Q: Applications of ZnO in organic and hybrid solar cells. Energy & Environmental Science. 2011, 4:3861-3877. 10.1039/c1ee01873f
12. Zhou X-Q, Hayat Z, Zhang D-D, et al.: Zinc oxide nanoparticles: synthesis, characterization, modification, and applications in food and agriculture. Processes. 2023, 11:1193. 10.3390/pr11041193
13. Satpal SB, Athawale AA: Synthesis of ZnO and Nd doped ZnO polyscales for removal of rhodamine 6G dye

under UV light irradiation. Materials Research Express. 2018, 5:085501. 10.1088/2053-1591/aad26c
14. ur Rehman F, Paker NP, ur Rehman S, Javed MT, Munis MFH, Chaudhary HJ: Zinc oxide nanoparticles: biogenesis and applications against phytopathogens. Journal of Plant Pathology. 2023, 106:45-65. 10.1007/s42161-023-01522-x
15. Sangareswari M, Meenakshi M: Development of efficiency improved polymer-modified TiO2 for the photocatalytic degradation of an organic dye from wastewater environment. Applied Water Science. 2015, 7:1781-1790. 10.1007/s13201-015-0351-6
16. Jadoun S, Yáñez J, Mansilla HD, Riaz U, Chauhan NPS: Conducting polymers/zinc oxide-based photocatalysts for environmental remediation: a review. Environmental Chemistry Letters. 2022, 20:2063-2083. 10.1007/s10311-022-01398-w
17. Lv Y, Wang L, Liu T, Liu H, Lv K, Zhang Y, Wu J: Study on photocatalytic properties of zinc oxide polypyrrole nanocomposites. Energy Reports. 2022, 8:405-411. 10.1016/j.egyr.2022.05.185
18. Chatterjee S, Patra AK, Bhaumik A, Nandi AK : Poly[3-(2-hydroxyethyl)-2,5-thienylene] grafted reduced graphene oxide: an efficient alternate material of TiO2 in dye sensitized solar cells. ChemComm. 2013, 49:4646-4648. 10.1039/c3cc40843d
19. Yan B, Wang Y, Jiang X, Liu K, Guo L: Flexible photocatalytic composite film of ZnO-microrods/polypyrrole. ACS Applied Materials & Interfaces. 2017, 9:29113–29119. 10.1021/acsami.7b08462
20. Satpal S, Bhopale A, Deshpande P, Athawale A: Fabrication of ZnO-functionalized polypyrrole microcomposite as a protective coating to enhance anticorrosion performance of low carbon mild steel. Journal of Applied Polymer Science. 2019, 48319:1-9. 10.1002/app.48319
21. Shao H, Qian X, Huang B: Fabrication of single-crystal ZnO nanorods and ZnS nanotubes through a simple ultrasonic chemical solution method. Materials Letters. 2007, 61:3639-3643. 10.1016/j.matlet.2006.12.005
22. Alves KGB, Felix JF, de Melo EF, dos Santos CG, Andrade CAS, de Melo CP: Characterization of ZnO/polyaniline nanocomposites prepared by using surfactant solutions as polymerization media. Journal of Applied Polymer Science. 2012, 125:141-147. 10.1002/app.35502
23. Raja K, Ramesh PS, Geetha D, Kokila T, Sathiyapriya R: Synthesis of structural and optical characterization of surfactant capped ZnO nanocrystalline. Spectrochimica Acta Part A: Molecular and Biomolecular Spectroscopy. 2015, 136:155-161. 10.1016/j.saa.2014.08.092
24. Valença DP, Alves KGB, De Melo CP, Bouchonneau N: Study of the efficiency of polypyrrole/ZnO nanocomposites as additives in anticorrosion coatings. Materials Research. 2015, 18:273-278. 10.1590/1516-1439.371614
25. Chougule MA, Pawar SG, Godse PR, Mulik RN, Sen S, Patil VB: Synthesis and characterization of polypyrrole (PPy) thin films. Soft Nanoscience Letters. 2011, 1:6-10. 10.4236/snl.2011.11002
26. Roy S, Mishra S, Yogi P, Saxena SK, Sagdeo PR, Kumar R: Synthesis of conducting polypyrrole-titanium oxide nanocomposite: Study of structural, optical and electrical properties. Journal of Inorganic and Organometallic Polymers and Materials. 2017, 27:257-263. 10.1007/s10904-017-0680-z
27. McGuire K, Pan ZW, Wang ZL, Milkie D, Menéndez J, Rao AM: Raman studies of semiconducting oxide nanobelts. Journal of Nanoscience and Nanotechnology. 2002, 2:499-502. 10.1166/jnn.2002.129
28. Biswas S, Drzal LT: Multilayered nanoarchitecture of graphene nanosheets and polypyrrole nanowires for high performance supercapacitor electrodes. Chemistry of Materials. 2010, 22:5667-5671. 10.1021/cm101132g
29. Mohan Kumar G, Madhan Kumar A, Ilanchezhiyan P, Kang TW: Fabrication of polypyrrole/ZnO nanowires based organic-inorganic hybrid p-n junctions. Journal of Materials Science: Materials in Electronics. 2015, 26:2384-2388. 10.1007/s10854-015-2695-y
30. Liwu Z, Hanyun C, Ruilong Z, Yongfa Z: Photocorrosion suppression of ZnO nanoparticles via hybridization with graphite-like carbon and enhanced photocatalytic activity. The Journal of Physical Chemistry C. 2009, 113:2368-2374. 10.1021/jp807778r
31. Hosseini MG, Bagheri R, Najjar R: Electropolymerization of polypyrrole and polypyrrole-ZnO nanocomposites on mild steel and its corrosion protection performance. Journal of Applied Polymer Science. 2011, 121:3159-3166. 10.1002/app.33952
32. Chen Y, Zhao Z, Zhang C: Structural and electrochemical study of polypyrrole/ZnO nanocomposites coating on nickel sheet synthesized by electrochemical method. Synthetic Metals. 2013, 163:51-56. 10.1016/j.synthmet.2012.12.013
33. Batool A, Kanwal F, Imran M, Jamil T, Siddiqi SA: Synthesis of polypyrrole/zinc oxide composites and study of their structural, thermal and electrical properties. Synthetic Metals. 2012, 161:2753-2758. 10.1016/j.synthmet.2011.10.016
34. Amorim SM, Steffen G, de S Junior JMN, Brusamarello CZ, Romio AP, Domenico MD: Synthesis, characterization, and application of polypyrrole/TiO2 composites in photocatalytic processes: A review. Polymers and Polymer Composites. 2020, 29:1055-1074. 10.1177/0967391120949489
35. Ovando-Medina VM, Lopez RG, Castillo-Reyes BE, Alonso-Davila PA, Martinez-Gutierrez H, González-Ortega O, Farias-Cepeda L: Composite of acicular rod-like ZnO nanoparticles and semiconducting polypyrrole photoactive under visible light irradiation for methylene blue dye photodegradation. Colloid and Polymer Science. 2015, 293:3459-3469. 10.1007/s00396-015-3717-2
36. Silvestri S, Dias Ferreira C, Oliveira V, Labrincha JMTB, Tobaldi DM: Synthesis of PPy-ZnO composite used as photocatalyst for the degradation of diclofenac under simulated solar irradiation. ACS Applied Materials & Interfaces. 2019, 375:261-269. 10.1016/j.jphotochem.2019.02.034
37. Ahmed A, Sabir S, Khan MZ: Zinc oxide-decorated polypyrrole/chitosan bionanocomposites with enhanced photocatalytic, antibacterial and anticancer performance. RSC Advances. 2019, 9:41135-41150. 10.1039/c9ra06493a
38. Nayebi P, Babamoradi M: Synthesis of ZnO nanorods/Fe3O4/polypyrrole nanocomposites for photocatalytic activity under the visible light irradiation. Optik. 2021, 244:167497. 10.1016/j.ijleo.2021.167497